

Elsevier Editorial(tm) for Advances in Space Research
Manuscript Draft

Manuscript Number:

Title: VELOCITY TOMOGRAPHY OF THE CORE OF THE CENTAURUS CLUSTER
COSPAR no: E1.2-0008-04

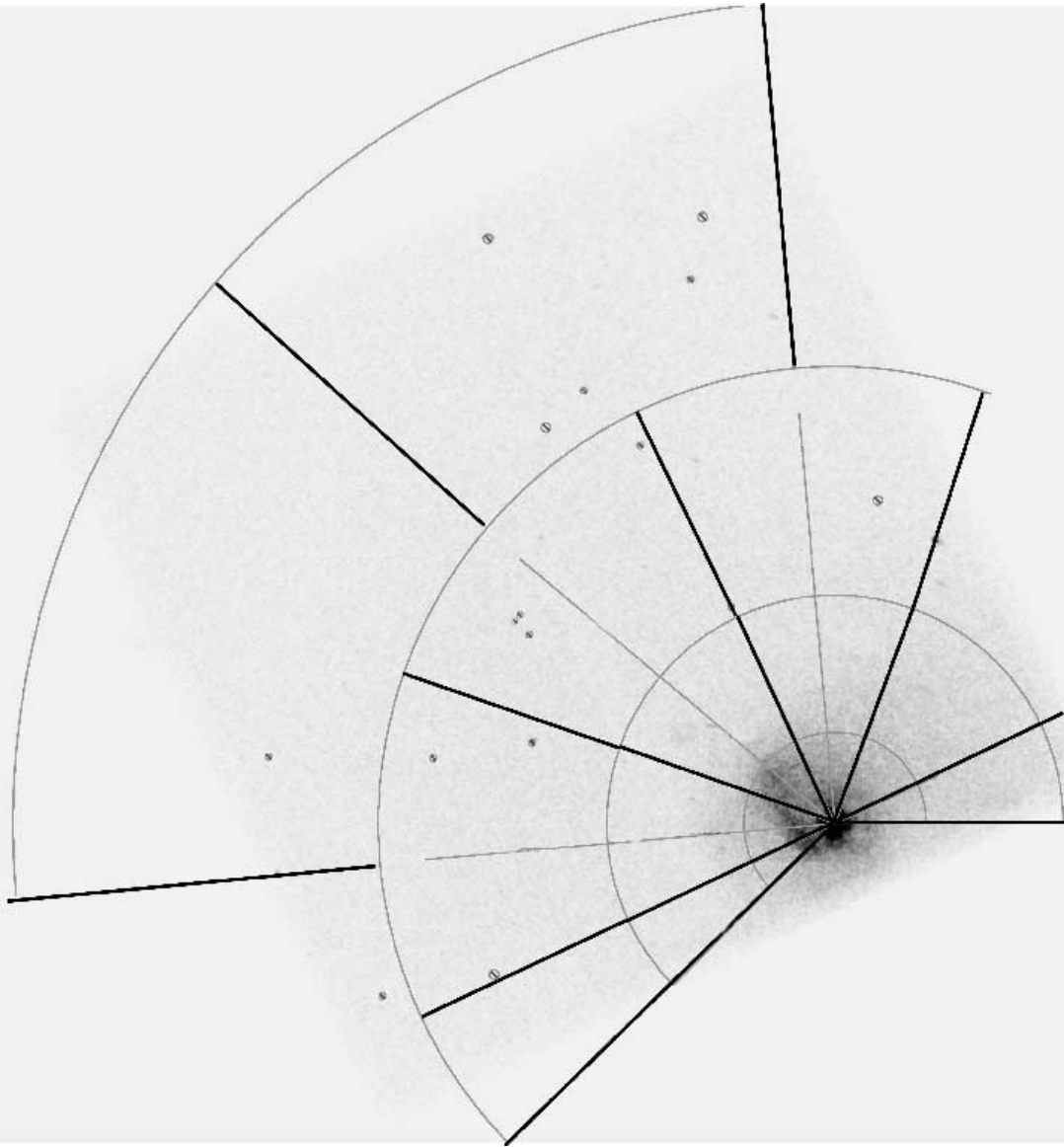
Article Type: Contributed Paper

Keywords: galaxies: clusters: Abell 3526; intergalactic medium; cooling flows; X-rays

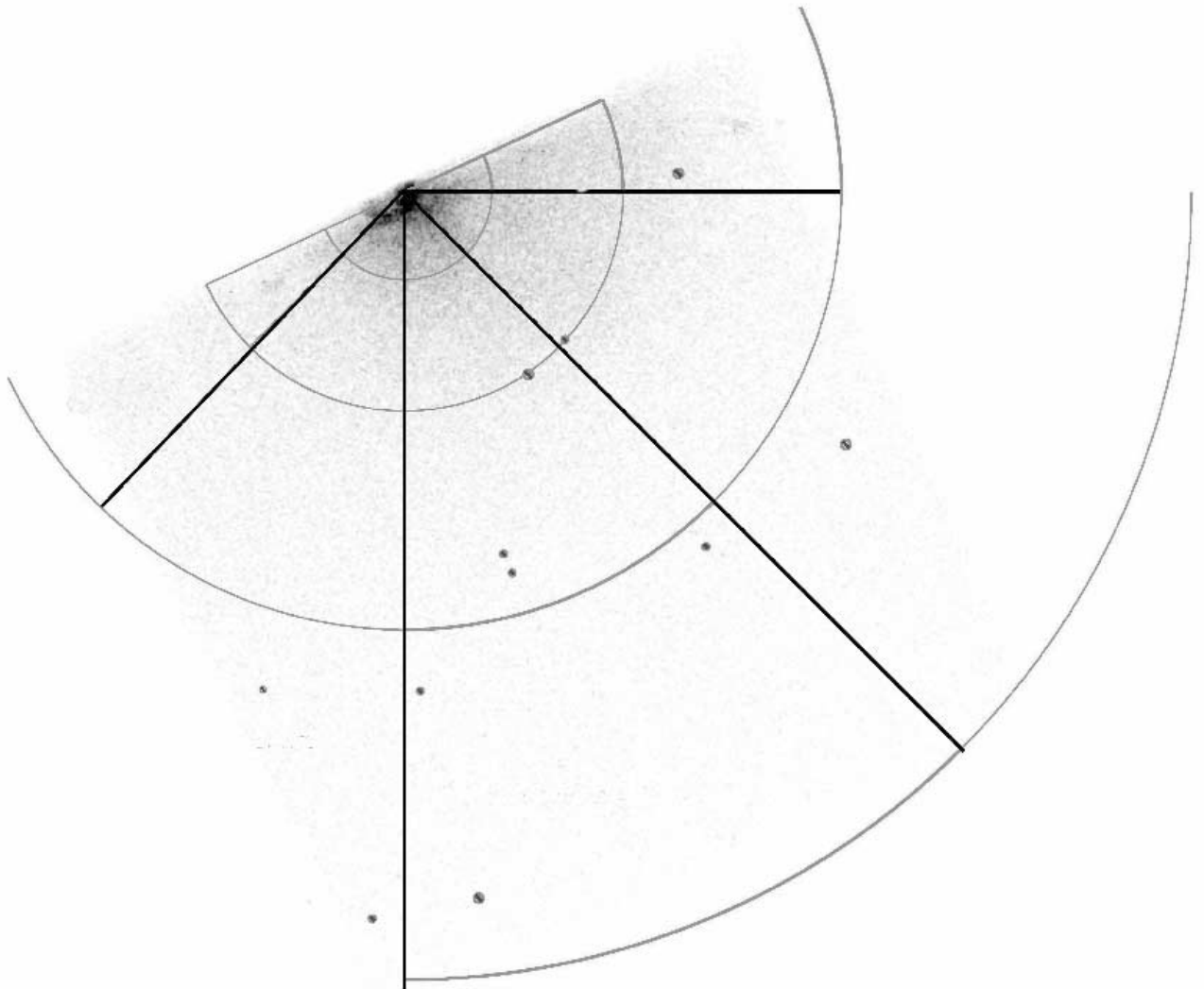
Corresponding Author: Dr renato A dupke University of Michigan

Other Authors: Joel Bregman, PhD University of Michigan

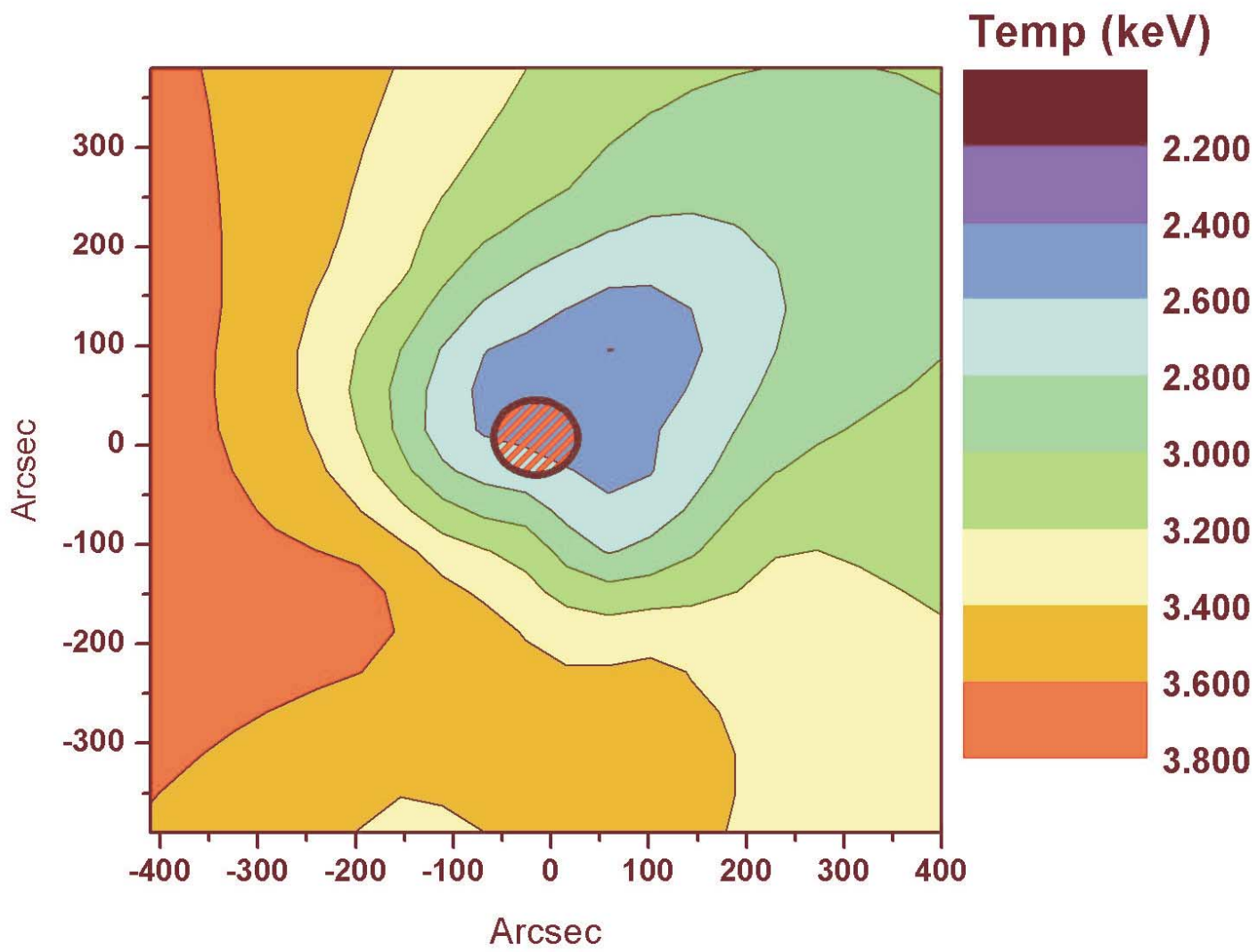
Figure



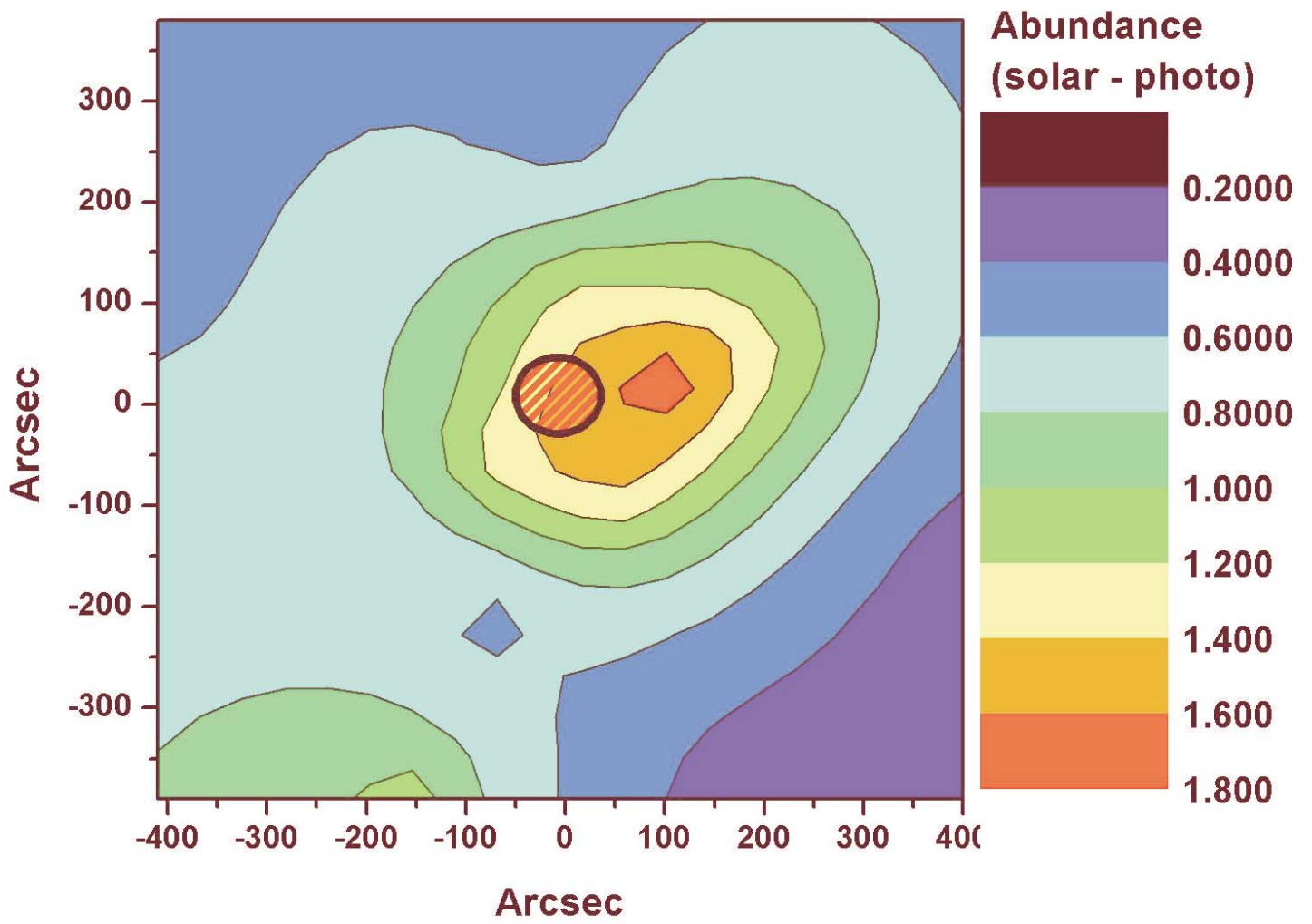
Figure



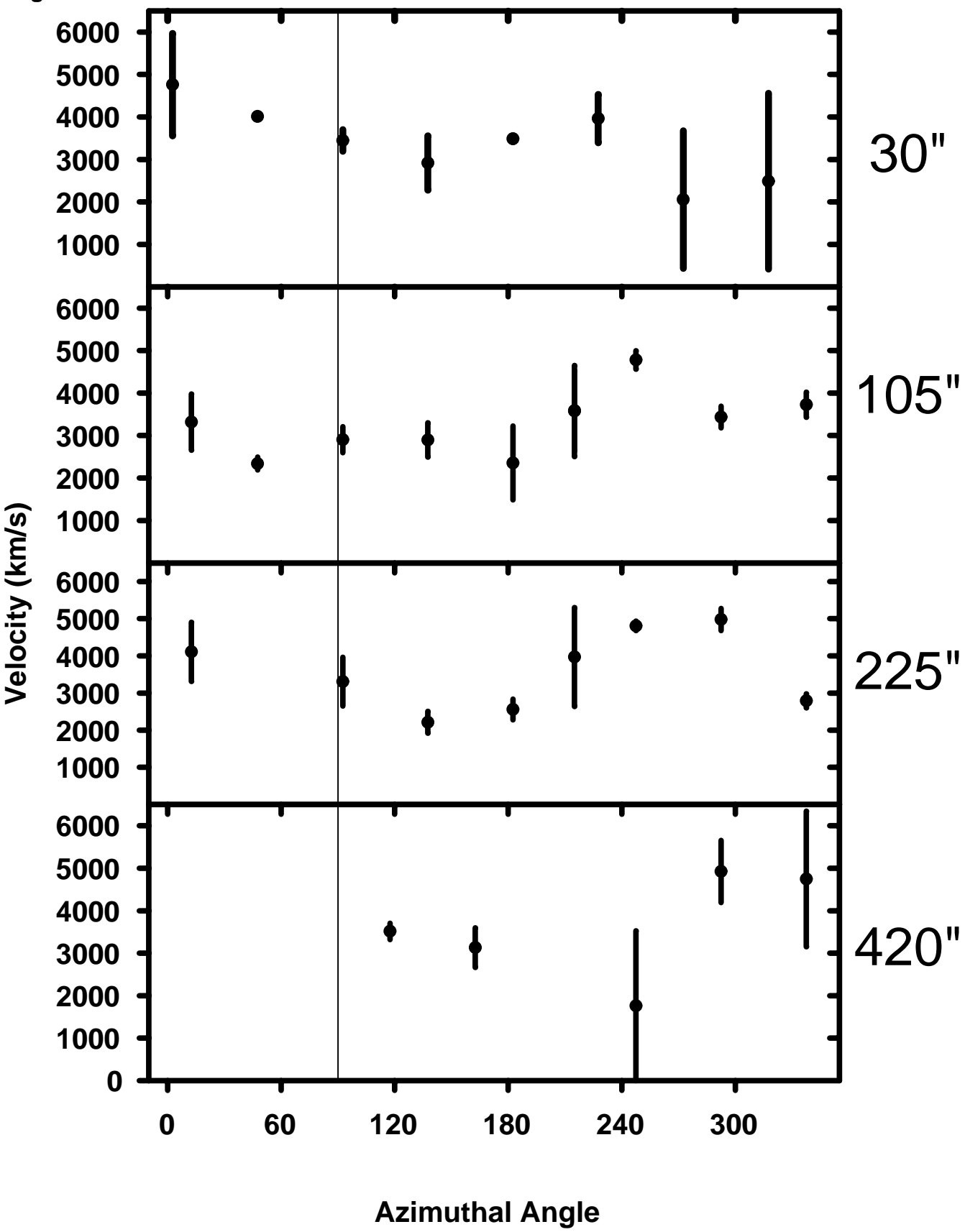
Figure



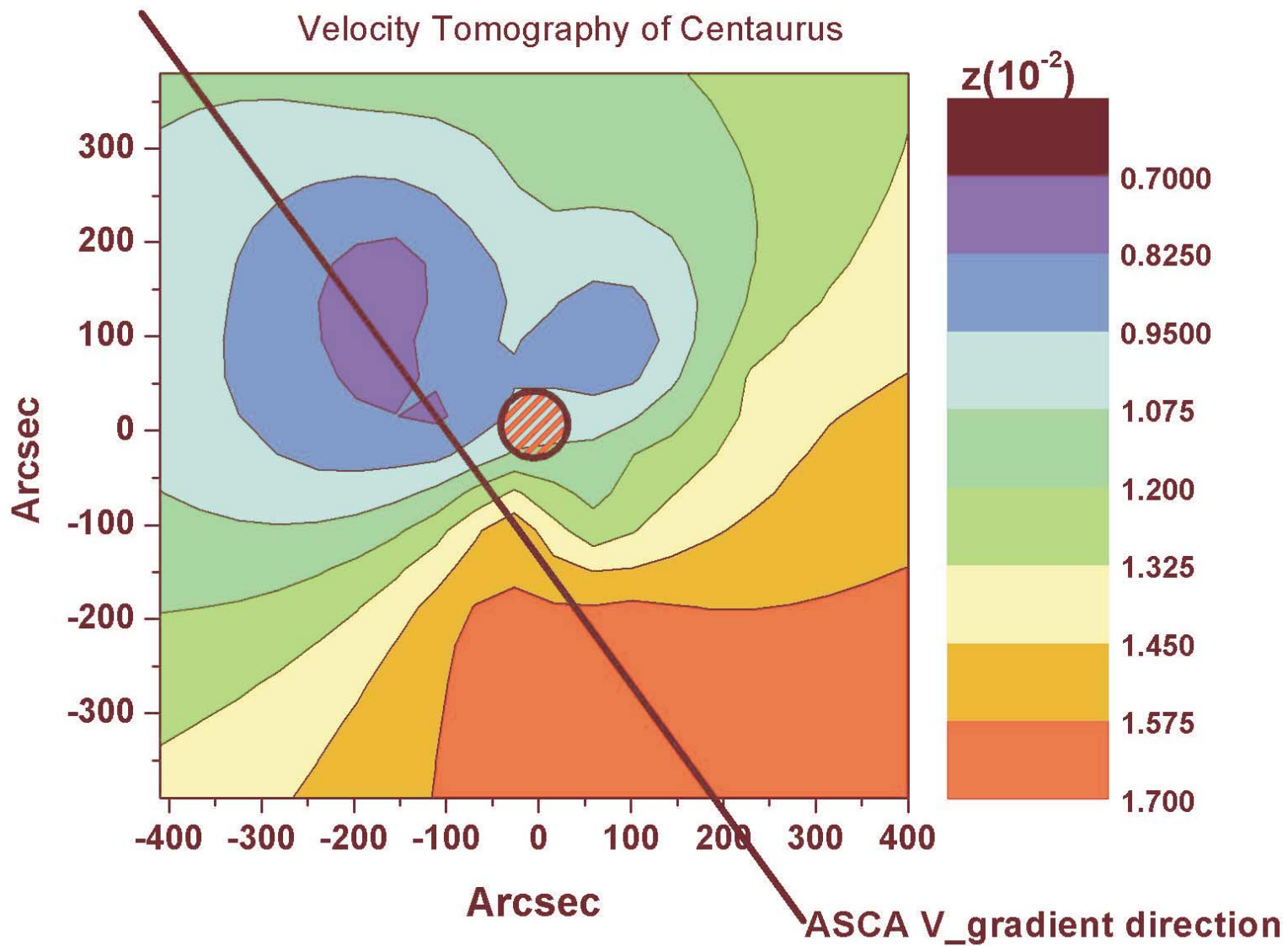
Figure



Figure



Figure



VELOCITY TOMOGRAPHY OF THE CORE OF THE CENTAURUS CLUSTER

Renato Dupke & Joel Bregman

Dept. Astronomy, University of Michigan, 830 Dennison, Ann Arbor 48109

Abstract

Previous *ASCA* analysis of the velocity distribution of the intracluster gas of the Centaurus cluster found velocity gradients on the order of >2000 km/s $3'-8'$ from the clusters' center. The gain variations across the spectrometers on-board *Chandra* are more than 3 times smaller than in *ASCA* SISs. Here, we present the preliminary results for a velocity analysis of the ICM of Centaurus at spatial scales smaller than $5'$ with *Chandra*'s ACIS-S3. This is the first observation specifically designed to reduce gain variations to a minimum and therefore to constrain ICM bulk velocities to <500 km/s reliably.

Keywords: galaxies: clusters: Abell 3526; intergalactic medium; cooling flows; X-rays

1- Introduction

Being the largest gravitationally bound systems in the universe, galaxy clusters can provide key information about structure formation and large-scale properties of the universe. For example, if they represent a “fair sample” of the early universe their baryonic mass fraction f_b should be equal to Ω_b/Ω_m , where Ω_b and Ω_m are the baryon and total mass densities of the universe normalized to the critical density (White et al 1993). This can be combined with Ω_b as predicted from light element abundances through big-bang nucleosynthesis (Schramm & Turner 1998) to provide constraints to Ω_m (Bahcall et al 1999 and references therein). Most of the baryonic mass of galaxy clusters is in the form of hot (10^{7-8} K) X-ray emitting diffuse highly ionized gas. Therefore, the precision with which the baryon fraction in clusters is estimated depends heavily on how well we can determine the gas mass, which in turn, depends on how well we know the physical state of the intracluster medium (ICM).

The primary process of formation and growth of galaxy clusters is the merging of collapsed subsystems, which creates strong temperature, density and gas velocity substructures (e.g. Ricker 1998). The latter is the least studied and potentially the most informative quantity to determine the gas dynamics. Off-center merging imparts angular momentum to the intracluster gas, which, according to recent numerical+hydro simulations, can last several Gyr (Gomez et al. 2002, Ricker et al. 1998, Takizawa 2000, Motl et al. 2004). The link between temperature substructure and the merger stage is often made by comparison with hydrodynamical simulations (e.g. Evrard 1990; Katz & White 1993; Roettiger, Burns & Loken 1993,1996; Pearce, Thomas & Couchman 1994; Navarro, Frenk & White 1995; Evrard, Metzler, & Navarro 1996; Roettiger, Loken & Burns 1997, Ricker 1998; Takizawa & Mineshige 1998; Takizawa 1999, 2000 and references therein).

The gas in clusters is not completely primordial (leftovers from galaxy formation). Rather a significant part of it was processed in stars, enriched with heavy elements and ejected back into the intracluster medium. This is inferred from the presence of “metal” emission lines in the X-ray spectra of galaxy clusters which show an average abundance of ~ 0.3 solar. This fact provides us with a unique opportunity to assess the gas dynamics by measuring the Doppler shift differences in the emission lines from spectra of the cluster gas

taken at different locations using X-ray spectrometers. The spectrometers on-board ASCA had originally an energy resolution (FWHM) of 2-4% (Solid-state Imaging Spectrometer or SIS) to 8% (Gas Imaging Spectrometer or GIS) at 5.9 keV. The situation is better for the Advanced CCD Imaging Spectrometer (ACIS) on-board *Chandra* ($3\% < \text{FWHM} < 3.6\%$ at 5.9 keV depending on the chip row¹) and also for the European Photon Imaging Cameras (EPICs) onboard *XMM* ($2.3\% < \text{FWHM} < 2.8\%$ at 5.9 keV).

The ability to measure intracluster gas velocities is not merely a matter of collecting sufficient numbers of photons. The most crucial issue is to know the instrumental gain (conversion of pulse-height to X-ray energy) variation to a precision greater than the velocities one is trying to measure. The main advantage of ASCA was the fact that the gain variations across the detectors (for all four spectrometers) were well known and its variations across the detectors could be properly taken into account. This is currently the case for *Chandra*, will be the case for *XMM* in the near future and is expected to be a small problem for the calorimeter on-board the future *ASTRO-E2* mission ($\sim 1\text{-}2$ eV across the frequency range, Figueroa, E. 2004, Personal Communication).

Dupke & Bregman (2001) found significant velocity gradients near the center of the Centaurus cluster using a deep ASCA observation of that cluster. The velocity gradient was detected independently with SIS 0 and SIS 1. The maximal velocity gradient was found to be $(3.3 \pm 1.1) \times 10^3$ km/s and did not show any clear correlation with the temperature or metal abundance gradients. *Chandra* provided us with the opportunity to minimize the effects of gain instability across the CCDs and therefore to verify and improve the results obtained with ASCA. We used two consecutive pointings of specific regions at the same CCD location, to minimize intrachip gain fluctuations. In this *proceedings* we present the results of a full scale mapping of the velocity distribution across the central $8'$ of the Centaurus cluster.

2- Data Reduction

Abell 3526 off-center pointings analyzed in this work were observed using Chandra ACIS-S3 in April 18th 2003, for 35ksec each. After removal of high background times we were left with 34.3 ksec & 33.9 ksec for the two pointings. In both cases the chip was centered on the regions of maximal departure from the systemic velocity as derived from a previous ASCA analysis (Dupke & Bregman 2001). The spatial configuration of the regions analyzed in this work and the relative location of the cluster's centers with respect to the ACIS-S3 chip is shown in Figures 1. The regions are PIE sectors around the cluster's core, which is excluded from the analysis. The reason for extracting the core off our analysis is that it is spectroscopically complex and its physical parameters have anisotropic distribution (Sanders & Fabian 2002), requiring the use of distinct multiple spectral components.

We used Ciao 3.0.2 with CALDB 2.28 to screen the data. The data were cleaned using the standard procedure described in cxc.harvard.edu/ciao/guides/acis_data.html. ACIS particle background was cleaned as prescribed for VFaint mode. A gain map correction was applied together with PHA and pixel randomization. Point sources were extracted and the background used in spectral fits was generated from blank-sky observations using the *acis_bkgnd_lookup* script. Here we show the results of spectral fittings with XSPEC V11.3.1 (Arnaud 1996) using the *mekal* thermal emission models. Metal abundances are measured relative to the solar photospheric values of Anders & Grevesse (1989). Galactic photoelectric absorption was incorporated using the *wabs* model (Morrison & McCammon

¹ asc.harvard.edu/cal/Links/Acis/acis/Cal_prods/eres/in_flight/plotneww123/plotneww123.html, ACIS Memo #181

1983). Spectral channels were grouped to have >20 counts/channel. Energy ranges were restricted to 0.5-9.5 keV.

The known reduction of quantum efficiency due to molecular contamination build up on optical blocking filter was corrected automatically within the *mkwarf* routine (Chartas G. 2004 Personal Communication). We noticed significant changes in the best-fit parameters (NH and temperature) for some overlapping regions near the CCD borders that are most likely due to improper automatic correction for a non-uniform QE degradation near the CCD borders (Vikhlinin 2004 Personal Communication). Here consider only fitting errors and assume that there is no intrachip gain variations. This is valid for the regions of maximum velocity discrepancy, which are in the center of the S3 chip. For the other regions the real uncertainties can be larger and a more elaborate correction for that will be carried out in a separate future work that will allow us to build a complete velocity map around the clusters core with significantly better accuracy (Dupke & Bregman 2005).

3 – Results & Summary

We present the temperature and metal abundance in Figures 2 & 3, respectively. Both distributions are anisotropic especially along the direction close to E-W, which coincides with the direction of the incoming Cen45 group, which centered in NGC4709 (Lucey et al. 1986a, b, Churazov 1999). In the regions displayed ($r>1'$) the gas temperatures vary from (2.32 ± 0.06) keV near the center to (3.72 ± 0.15) keV, $7'$ away from the center towards the E direction. The temperature within the central arcminute varies from (1.24 ± 0.02) keV to (1.68 ± 0.03) keV, consistent with the double temperature model fittings used by Sanders & Fabian (2002), who analyzed the cluster's core in great detail.

The metal abundance distribution shows an overall increase towards the center but also has an anisotropic distribution peaking at (1.81 ± 0.28) Solar (photospheric) towards the W (Figure 3). It declines radially and the gradient is steepest towards the SW, where it achieves values as small as (0.29 ± 0.07) Solar. Within the core the metal abundances are also anisotropic but the overall values are sub-solar.

The azimuthal velocity distributions are shown in Figure 4 as a function of average distance from the cluster's center. North is indicated by a vertical line. The regions where the velocity gradients are seen to be strongest are between the regions centered at 137.5° - 182.5° , where the velocity is found to be $(2.4\pm0.3) \times 10^3$ km/s versus the regions centered at 247.5° - 292.5° where the best-fit velocities are significantly higher $(4.9\pm0.2) \times 10^3$ km/s. This is especially obvious in the distribution corresponding to a radial distance of $225''$ from the center, although the velocity gradient is also seen but with lower significance at radial distances $105''$ and $420''$. The velocity map is shown in Figure 5 (the central arcmin is excluded). If the velocity distribution is a result of gas circulation the rotational velocities are $\sim 1,200$ km/s implying that a significant fraction of the ICM energy ($>50\%$) can be kinetic, even in clusters where there are no strong signs of merging. The direction of maximum velocity gradient is found to be roughly perpendicular to that of the incoming Cen45 suggesting that the observed gas bulk flows pre-existed the current merging event.

Acknowledgments: We would like to thank Catherine Grant, George Chartas, Alexey Vikhlinin for helpful discussions. We acknowledge support from NASA Grant NAG 5-3247. This research made use of the HEASARC ASCA database and NED.

References

- Anders, E., & Grevesse N. 1989, *Geochimica et Cosmochimica Acta*, 53, 197
- Arnaud, K. A. 1996, in *ADASS V*, ASP Conf. Series vol101, eds. Jacoby, G., & Barnes, J., p.17
- Bahcall et al.,1999, *Science*, 284 148
- Churazov, E., Gilfanov, M., Forman, W., & Jones, C. 1999, *ApJ*, 520, 105
- Churazov, E., Gilfanov, M., Forman, W., and Jones, C. 1999, *ApJ*, 520, 105
- Dupke, R.A. & Bregman, J. N. 2001, *ApJ*, 547, 705
- Dupke, R.A. & Bregman, J. N. 2005, *ApJL*, to be Submitted
- Evrard, A. E. 1990, *ApJ*, 363, 349;
- Evrard, A. E., Metzler, C. A., & Navarro, J. F. 1996, *ApJ*, 469, 494;
- Katz, N., & White, S. D. M. 1993, *ApJ*, 412, 455;
- Lucey, J. R.; Currie, M. J.; Dickens, R. J. 1986a, *MNRAS*, 221, 453
_____, 1986b, *MNRAS*, 222, 427
- Morrison, R., & McCammon, D. 1983, *ApJ*, 270, 119
- Motl, P. M., Burns, J. O., Loken, C., Norman, M. L., Bryan, G. 2004, *ApJ*, 606, 635
- Navarro, J. F., Frenk, C. S., & White, S. D. M. 1995 *MNRAS*, 275, 720
- Pearce, F. R., Thomas, P. A., & Couchman, H. M. P. 1994, *MNRAS*, 268,953;
- Ricker, P. M. 1998, *ApJ*, 496, 670
- Roettiger, K., Burns, J. O., & Loken, C. 1993, *ApJL*, 407, 53;
- Roettiger, K., Burns, J. O., & Loken, C. 1996, *ApJ*, 473, 651
- Roettiger, K., Loken, C., & Burns, J. O. 1997, *ApJS*, 109, 307
- Sanders, J. & Fabian, A. 2002, *MNRAS*, 331, 273
- Schramm, D. & Turner, M. 1998, *Rev. Mod. Phys.* 70, 303
- Takizawa, M., & Mineshige, S. 1998, *ApJ*, 499, 82;
- Takizawa, M. 1999, *ApJ*, 520,514
- Takizawa, M. 2000, *ApJ*, 532, 183
- White, S. D. M., Navarro, J. F., Evrard, A. E. & Frenk, C. S. 1993, *Nature* 366, 429

Figure Caption 1: Spatial configuration of the regions selected for spectral analysis in this work.

Figure Caption 2: Temperature map of the Centaurus cluster. The region within the central arcminute is excluded from the analysis.

Figure Caption 3: Metal abundance map of the Centaurus cluster. The region within the central arcminute is excluded from the analysis.

Figure Caption 4: Azimuthal distribution of Velocities for different radial distances (indicated on the right). The North direction is indicated by the vertical line.

Figure Caption 5: Redshift map of the Centaurus cluster. The units in the scale are in 0.01. The black line shows the direction of maximum velocity gradient as found in a previous work using *ASCA* data. The region within the central arcminute is excluded from the analysis.